



Nanoscale

Facile alkali metal hydroxide-assisted controlled and targeted synthesis of 1T MoS₂ single crystal nanosheets for lithium ion battery anodes

Journal:	<i>Nanoscale</i>
Manuscript ID	NR-ART-05-2019-004537.R1
Article Type:	Paper
Date Submitted by the Author:	02-Jul-2019
Complete List of Authors:	Li, Zhao; Northwestern Polytechnical University School of Natural and Applied Sciences Zhan, Xun ; University of Illinois at Urbana-Champaign Department of Materials Science and Engineering, DEPARTMENT OF MATERIALS SCIENCE AND ENGINEERING Qi, shuhua; Northwestern Polytechnical University School of Natural and Applied Sciences

SCHOLARONE™
Manuscripts



Received 00th January 20xx,

Facile alkali metal hydroxide-assisted controlled and targeted synthesis of 1T MoS₂ single crystal nanosheets for lithium ion battery anodes

Accepted 00th January 20xx

DOI: 10.1039/x0xx00000x

www.rsc.org/Zhao Li,^{a,b} Xun Zhan^b and Shuhua Qi^{a*}

High-quality metallic 1T phase MoS₂ single crystal nanosheets were synthesized by facile eco-friendly alkali metal hydroxide-assisted controlled and targeted approach via calcination of lithium hydroxide and ammonium tetrathiomolybdate under argon atmosphere at 1000 °C. 1T MoS₂ single crystal nanosheets were used as lithium-ion battery anodes, presenting superior electrochemical performances including long cycle life and high capacities. The first charge and discharge capacities are up to 889.1 mAh g⁻¹ and 892.5 mAh g⁻¹, respectively, giving a first cycle coulombic efficiency of 98.0% which increases to greater than 99.1% in the second cycle. In 400th cycle, charge and discharge capacities are 737.2 mAh g⁻¹ and 738.0 mAh g⁻¹, respectively, with 82.9% capacity retention ratio. The work not only provides a novel strategy for fabricating metallic 1T phase MoS₂ which are used as lithium ion battery anodes but introduce a facile eco-friendly lithium hydroxide-assisted controlled and targeted approach for different phase MoS₂ (1T and 2H), also it can be extended to other alkali metal hydroxide-assisted (NaOH, KOH) approaches for MoS₂ preparation.

1. Introduction

Transitional metal dichalcogenides (TMDs), as a kind of two-dimensional (2D) graphene-like materials, have attracted much attention in lithium/sodium battery system, supercapacitor and catalytic hydrogen evolution due to their unique and fascinating physical and chemical properties.¹⁻⁷ As the most typical family member of TMDs, molybdenum disulfide (MoS₂) is a representative layer material in which each layer is composed of Mo atom sandwiched between two S atom.⁸ The adjacent layers are connected through van der Waals interactions.⁹ MoS₂ has two kinds of phase structure with distinct symmetries, the 2H (trigonal

prismatic D_{3h}) and 1T (octahedral O_h) phases (Fig. 1a, b),^{10,11} in which its metallic 1T phase has high electrical conductivity (10-100 S cm⁻¹) and provides fast ion diffusion between the nanosheets.¹²⁻¹⁴

Compared with 2H MoS₂, metallic 1T phase MoS₂ is a metastable structure which encountered some difficulties on its fabrication.¹⁵ At present, versatile approaches were introduced to overcome the problem.¹⁶⁻¹⁸ In general, two strategies have been introduced to fabricate 1T phase MoS₂ nanosheets: i) top-down approach which is rely on the reversible transition reaction from 2H phase to 1T phase because of the dominant and stable structure of 2H phase in nature.¹⁹⁻²¹ The 1T phase MoS₂ is usually achieved by chemical/electrochemical intercalation with alkali metal ions (Li⁺, Na⁺, and K⁺), especially organolithium (such as butyllithium) which is liable to react with moisture and oxygen at room temperature. More importantly, the obtained metallic 1T phase MoS₂ is easy to restack to form 2H phase MoS₂ over 95 °C;²² ii) bottom-up approaches are efficient routes to directly synthesize 1T phase

a. School of Natural and Applied Sciences, Northwestern Polytechnical University, Xi'an, Shaanxi 710072, China. E-mail: qishuhuanwpu@163.com

b. Department of Materials Science and Engineering, Frederick Seitz Materials Research Laboratory, and Beckman Institute for Advanced Science and Technology, University of Illinois at Urbana-Champaign, Urbana, Illinois 61801, United States.

Electronic Supplementary Information (ESI) available: [details of any supplementary information available should be included here]. See DOI: 10.1039/x0xx00000x

MoS₂ which is based on the hydrothermal/solvothermal growth in the presence of Mo and S molecular precursors.²³⁻²⁵ Also, in traditional MoS₂ preparation, the ammonium tetrathiomolybdate was directly calcination under high temperature, releasing the hydrogen sulfide gas, which is harmful for the environment.^{26,27}

To address this issue, we introduce a facile eco-friendly alkali metal hydroxide-assisted controlled and targeted strategy for fabricating high quality stable metallic 1T MoS₂ single crystal nanosheets by calcination of lithium hydroxide and ammonium tetrathiomolybdate (MoS₂ precursor) at 1000 °C under argon gas. Hydroxide ion (OH⁻) in lithium hydroxide can react with intermediate products of ammonium tetrathiomolybdate (ammonium sulfide, (NH₄)₂S), avoiding release of hydrogen sulfide gas during the direct calcination of ammonium thiomolybdate in previous MoS₂ preparation. In order to compare performances of the distinct phase MoS₂ (1T and 2H), the controlled and targeted synthesis of 1T phase MoS₂ and 2H phase MoS₂ can be realized by different calcination temperature (1000 °C and 400 °C) under argon gas, respectively, avoiding the dependence on the rigorous and dangerous solvent, complicated strategy and the high risk of using dangerous butyllithium as reagent in previous work.²⁸ The 1T MoS₂ single crystal nanosheets were used as lithium ion battery anodes, presenting high first specific charge and discharge capacity of 889.1 mAh g⁻¹ and 892.5 mAh g⁻¹ respectively, giving a first cycle coulombic efficiency of 98.0% which increases to greater than 99.1% in the second cycle. In 400th cycle, the charge and discharge capacities are still 737.2 mAh g⁻¹ and 738.0 mAh g⁻¹, respectively. This strategy provides a facile eco-friendly lithium hydroxide-assisted controlled and targeted approach for 1T and 2H phase MoS₂, also can be extended to other alkali metal hydroxide-assisted (NaOH, KOH) approaches for fabricating different phase MoS₂.

2. Experimental section

2.1 Synthesis of metallic 1T MoS₂ single crystal nanosheets

First, 1 mmol LiOH•H₂O and 0.5 mmol (NH₄)₂MoS₄ were added into 1.5 mL Millipore water (18.2 MΩ cm resistivity) to form the LiOH/(NH₄)₂MoS₄ precursor. Second, the precursor was transferred into a porcelain combustion boat which was placed in the centre of a mullite tube which was placed in a horizontal tube furnace. The precursor was heated at 85 °C for 4 hours to remove the water from the precursor. Afterwards, the temperature of tube furnace

was raised to 1000 °C within 3 hours and kept for 5 hours, which was subsequently cooled down to the room temperature naturally after calcination process. Finally, the samples were washed with DI water for 30 minutes at 5000 rpm, and then were centrifuged with ethyl alcohol for 30 minutes at 15000 rpm to remove the precipitate. The samples were dried under vacuum oven at 60 °C for 12 hours, finally the samples were collected for later use. The schematic was shown in Fig. 1c.

2.2 Materials characterization

X-ray photoelectron spectroscopy (XPS) spectra of 1T MoS₂ were collected with a Kratos Axis Ultra XPS system with a monochromatic Al Kα (1486.6eV) source, and the binding energy scale was calibrated using the aliphatic C 1s peak (284.8 eV). The Nanophoton Raman-11 system was employed to measure Raman data using 532 nm laser excitation. The laser exposure time is 30 seconds at a power of 1.30 mW. High-resolution transmission electron microscopy (HRTEM) studies and selected area electron diffraction were performed on a JEOL 2100 cryo TEM operating at 200 kV. X-ray diffraction (XRD) was collected using Philips X'pert MRD XRD with Cu Kα radiation (1.5418 Å). Observed XRD peaks were compared with the Joint Committee on Powder Diffraction Standards. The 1T MoS₂ morphologies were measured using Hitachi S-4800 scanning electron microscopy (SEM) at 10 kV and 10 mA.

2.3 Electrochemical measurement

The 2032-type coin cells were assembled to measure the electrochemical properties on Princeton Applied Research Model 273A. The slurry consisting of 1T MoS₂ single crystal nanosheets, sodium alginates and carbon black (>99%, super-P; Alfa) with the mass ratio of 8:1:1 in Millipore water was processed into 120 μm thick electrode film on copper, then drying at 80 °C in a vacuum oven overnight, which was used as working electrode. 1 M LiPF₆ dissolved in a 50:50 (w/w) mixture of ethylene carbonate and diethyl carbonate was used as an electrolyte, a polypropylene microporous film was employed as the separator, lithium foil was used as counter and reference electrode, all cells were assembled in glove box. Galvanostatic tests were performed between 0.01 and 3.0 V versus Li/Li⁺. The cyclic voltammetry (CV) curves were measured over the potential range of 0.01-3V (vs. Li/Li⁺) at the scan rate of 0.1 mV s⁻¹. The C-rates were changed from 0.5 C, 1 C, 2 C, 5

C and 10 C, and back to 0.5 C, and each measurement was cycled 10 times.

3. Results and discussion

Two representative crystal phases of MoS₂ are discovered, one is the thermodynamically stable 2H phase (space group, P6₃/mmc) and the metastable 1T phase (space group, P $\bar{3}$ m1), respectively. In 2H phase MoS₂, H represent the hexagonal symmetry of the crystal structure, while T represents the trigonal symmetry of crystal structure.²⁹ Fig 1a shows the top-view and side-view crystal structure of 2H phase MoS₂, each Mo atom is surrounded by six S atoms, while the S atoms in the upper layer are directly lying on those of the lower layer, whereas in the 1T phase MoS₂ in Fig. 1b, the Mo atom is octahedrally coordinated to six neighboring S atoms, and the two S layers can be stacked into the A-B model.³⁰ Distinct electronic properties between 2H and 1T phase MoS₂ are discovered, which are attributed to the difference in crystal symmetry.^{31–33} Fig. 1c presents the schematic for the fabrication of high quality metallic 1T MoS₂ single crystal nanosheets and 2H phase MoS₂. The detailed chemical reaction is shown in Fig. S1(Supporting Information).

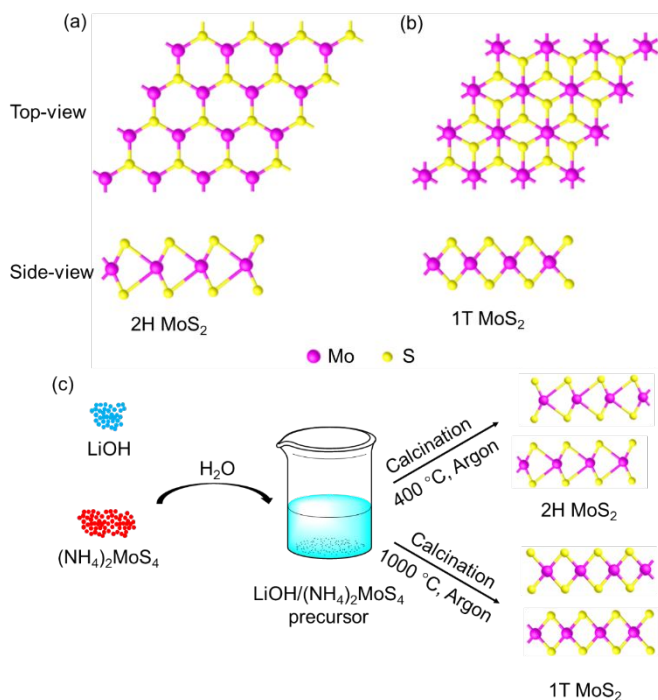


Fig. 1 Top-view and side-view crystal structure schematic illustration of (a) 2H phase MoS₂ and (b) 1T phase MoS₂. (c) Schematic for the fabrication of high quality metallic 1T MoS₂ single crystal nanosheets and 2H MoS₂.

In order to visually distinguish difference between the 1T and 2H phase MoS₂, the real photograph is introduced in Fig. 2a. The same amount of calcined 1T MoS₂ and 2H MoS₂ are added into the DI water to form the solution, which present the yellow green and black brown, respectively. To verify the 1T phase MoS₂, XRD is employed to characterize the crystal structure. A strongest peak at around 14.4° in Fig. 2b is observed, corresponding to the (002) crystallographic plane of 1T MoS₂, which interplanar spacing is 6.15 Å (PDF from JCPDS file number: 04-017-0898).³⁴ Interestingly, another new peak (001) at $2\theta=7.5^\circ$ is observed, indicating an additional separation between layer during the calcination. Other peaks at 15.7°, 21.4°, 29.0°, 33.2°, 40.4°, 44.2°, 58.3° and 60.5° are corresponded to the crystallographic planes of (100), (011), (004), (012), (11-2), (006), (22-1) and (008), respectively. In 2H MoS₂ XRD patterns, the strongest peak at 14.1° are assigned to the crystallographic planes of (002), other peaks at 32.6°, 39.5° and 58.3° are corresponded to the crystallographic planes of (100), (103) and (110), respectively. More importantly, the (002) peaks of 1T MoS₂ (Fig. 2c) are shifted higher than that of 2H MoS₂, consist with their crystal structures.³⁵

The XPS technique is an efficient approach to evaluate the chemical composition of 1T and 2H MoS₂. Fig. 2d is high-resolution XPS spectra of the 1T MoS₂ nanosheets. Two peaks at around 228.5 eV and 231.6 eV are corresponded to the binding energies of 3d_{5/2} and 3d_{3/2} for 1T phase MoS₂, which are resulted from Mo-S bonding in 1T MoS₂ single crystal nanosheets.^{36,37} 230.7 eV and 232.5 eV are binding energies of 3d_{5/2} and 3d_{3/2} for 2H phase MoS₂, respectively.

The peak at 225.5 eV, is consistent with S 2s, likely coming from the 1T MoS₂. Similarly, the S 2p XPS spectrum (Supporting information Fig. S2) consist of two peaks at around 161.5 eV and 162.5 eV which are also ≈ 1 eV lower than the peaks in 2H MoS₂ according to the literature, are associated with S 2p_{3/2} and S 2p_{1/2}, respectively, further confirming the presence of Mo-S bonding.³⁸ Furthermore, the composition (91.6% 1T phase and 8.4% 2H phase) obtained from those XPS peaks quantitative calculation indicated that the MoS₂ mainly consists of 1T phase MoS₂ nanosheets.

Raman spectroscopy is introduced to confirm that the 1T-phase MoS₂ could be obtained when the calcination temperature was raised to over 1000 °C. Fig. 2e is also employed to further verify crystal phase of 1T MoS₂, showing characteristic peaks at 283 cm⁻¹, 378 cm⁻¹ and 405 cm⁻¹, which are derived from the in-plane mode

and the out-of-plane mode (Fig. 2g).³⁹ The in-plane E_{2g}^1 mode results from opposite vibration of two S atoms with respect to the Mo atom while the A_{1g} mode is associated with the out-of-plane vibration of only S atoms in opposite directions.⁴⁰ Peaks at 147 cm^{-1} (J_1), 198 cm^{-1} (J_2) and 336 cm^{-1} (J_3) are attributed to Mo-Mo stretching vibrations and the superlattice in 1T MoS₂, providing direct evidence that distinguish 1T phase MoS₂ from 2H phase MoS₂.^{41,42} To distinguish the 1T phase MoS₂ and 2H phase MoS₂, 2H phase MoS₂ are obtained at $400\text{ }^\circ\text{C}$ calcination temperature, its Raman spectrum is shown in Fig. 2f. Obviously, three typical peaks at 408 cm^{-1} , 382 cm^{-1} and 286 cm^{-1} are attributed to in-plane mode and the out-of-plane mode, which are similar with 1T MoS₂.^{43,44} Fig. 2g illustrates the E_{1g} , E_{2g}^1 and A_{1g} vibration modes located at 283 cm^{-1} , 378 cm^{-1} and 404 cm^{-1} in 1T phase MoS₂, respectively, which are also corresponding to the vibration modes located at 286 cm^{-1} , 382 cm^{-1} and 408 cm^{-1} in 2H phase MoS₂, respectively.⁴⁵ The phase stability is of significance for 1T MoS₂, thus the Raman tests (Supporting information, Fig. S3 and Fig. S4) after 60 days and 90 days were introduced to evaluate the its stability. The results showed that all of characteristic peaks for 1T phase are existed, indicating the excellent stability.

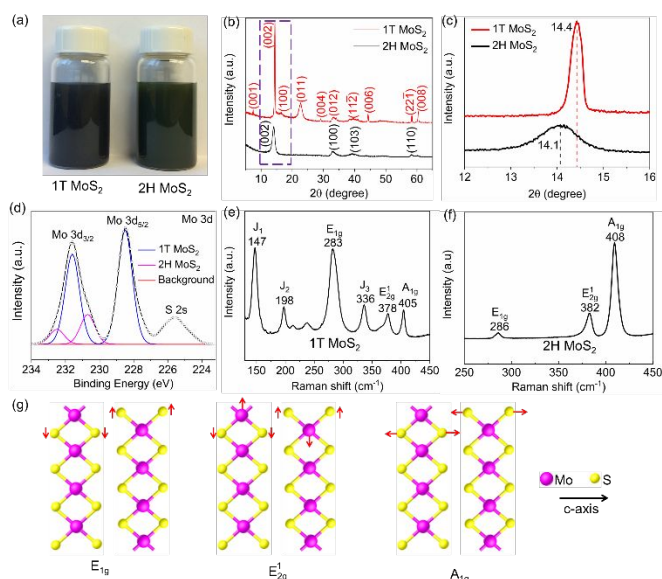


Fig. 2 (a) Real photograph of 1T and 2H MoS₂ dispersed in ethyl alcohol. (b) XRD patterns of 1T MoS₂ nanosheets. (c) Magnified XRD patterns of the (002) peaks of 1T and 2H-MoS₂ crystals, from the purple dashed area in b. (d) High-resolution XPS spectra of (c) Mo 3d, S 2s core-level peaks after Shirley background subtraction (red line is background curve) of 1T MoS₂ single crystal nanosheets.

The line with the circle symbol is the total curve for Mo 3d, other colors (green, blue and purple) lines are curves after peak-differentiating and fitting. Raman characterization of (e) 1T MoS₂ single crystal nanosheets and (f) 2H MoS₂. (g) Atomic vibration direction of E_{1g} , E_{2g}^1 and A_{1g} Raman modes of MoS₂.

Fig. 3a is the typical morphology of 1T MoS₂, observed by SEM. The 1T MoS₂ contains flake shaped nanosheets, with the average diameter of $\sim 500\text{ nm}$. Fig. 3b is the TEM bright field image of single nanosheet. The corresponding selective area electron diffraction is shown in Fig. 3c. Each nanoparticle is a single crystal, as seen in the sharp and unique set of diffraction pattern along [001] zone axis. This excellent crystallinity is also confirmed by HRTEM, shown in Fig. 3d.

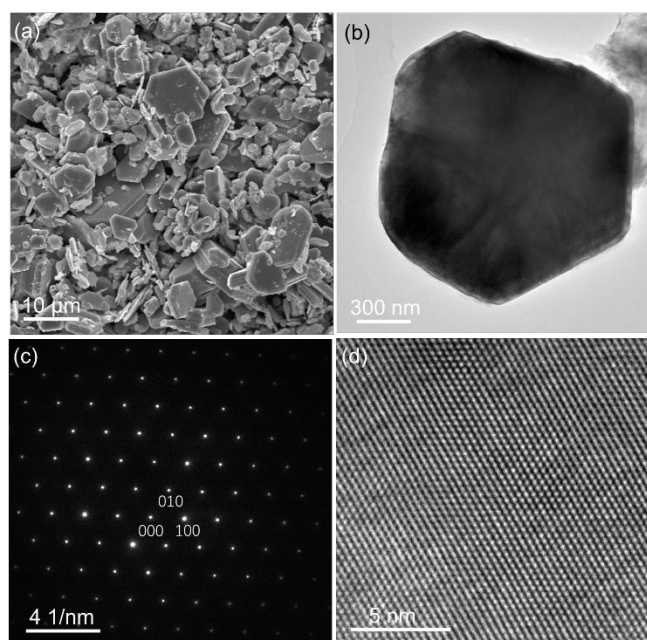


Fig. 3 SEM and TEM characterization of 1T phase MoS₂ single crystal nanosheets: (a) low-magnification of SEM image, (b) TEM bright field image, (c) selected area electron diffraction (SAED) image based on panel c, (d) high-resolution TEM image.

Fig. 4 presents the electrochemical performances of 1T MoS₂ electrode in lithium ion battery. Fig. 4a shows initial three cycles CV curves, in the first cycle, it is observed that a cathodic peak at 0.5 V , which is due to the conversion of Li_xMoS_2 to Mo particles and Li_2S , the formation of solid-electrolyte interphase (SEI) film. Another reduction peak at 0.93 V is assigned to lithium insertion into interlayer of 1T MoS₂ to form the Li_xMoS_2 .⁴⁶ In the following anodic scan, an anodic peak at 1.48 V is observed, which corresponds to the oxidation of Mo metal, another anodic peak at 2.28 V is due to

the oxidation of Li_2S . During the subsequent cathodic sweep, the peaks located at 0.93 and 0.46 V disappear, but there are three new peaks at 1.94, 1.10 and 0.24 V, manifesting that the lithiation and delithiation reaction of MoS_2 are an irreversible process.⁴⁷

In order to evaluate the rate performances of 1T MoS_2 electrodes, the cycling at 0.5 C, 1 C, 2 C, 5 C and 10 C were conducted. In Fig. 4b, electrodes exhibit charge and discharge of 890.5 mAh g^{-1} and 894.2 mAh g^{-1} at 0.5 C, 839.7 mAh g^{-1} and 842.2 mAh g^{-1} at 1 C, 760.9 mAh g^{-1} and 764.1 mAh g^{-1} at 2 C, 680.3 mAh g^{-1} and 685.2 mAh g^{-1} at 5 C, 586.3 mAh g^{-1} and 588.7 mAh g^{-1} at 10 C, respectively, and return to 875.8 mAh g^{-1} and 882.0 mAh g^{-1} at 0.5 C. The results indicate the superior rate capability of 1T MoS_2 single crystal nanosheets lithium-ion battery anodes.

Galvanostatic charge-discharge curves in Fig. 4c indicates the first charge and discharge capacities of 889.1 mAh g^{-1} and 892.5 mAh g^{-1} , respectively, giving a first cycle coulombic efficiency of 98.0% which increases to greater than 99.1% in the second cycle. In 10th cycle, the charge and discharge capacities are still 880.5 mAh g^{-1} and 885.2 mAh g^{-1} , maintaining high capacities and indicating the capacities decay slowly. Galvanostatic charge-discharge curves in Fig. 4d and cycling capacity with coulombic efficiency in Fig. 4e are employed to illustrate the cycling stability. The first charge and discharge capacities of 889.1 mAh g^{-1} and 892.5 mAh g^{-1} decrease to 835.6 mAh g^{-1} and 839.1 mAh g^{-1} after 100 cycles, respectively. In 200th cycle, the charge and discharge capacities are still remain on 797.5 mAh g^{-1} and 798.8 mAh g^{-1} , respectively. Even in 400th cycle, 737.2 mAh g^{-1} and 738.0 mAh g^{-1} are also obtained, respectively, with 82.9% capacity retention rate. In order to further demonstrate excellent cyclic performance of 1T MoS_2 electrode, the cyclic performance of 2H MoS_2 electrode was conducted and shown in Fig. S5 (supporting information) The first charge and discharge capacities of 744.6 mAh g^{-1} and 758.3 mAh g^{-1} decrease to 635.6 mAh g^{-1} and 637.8 mAh g^{-1} after 100 cycles, respectively, which are lower than that of 1T MoS_2 electrode.

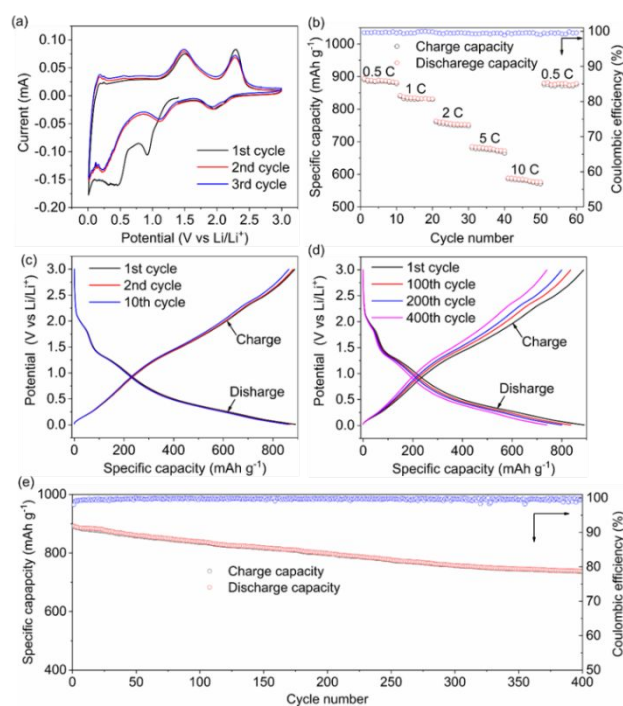


Fig. 4 Electrochemical performances of the 1T MoS_2 electrode: (a) CV curves of initial three cycles over the potential range of 0.01-3V vs Li/Li^+ . (b) Rate performances during cycling from 0.5 C to 10 C. Galvanostatic charge-discharge curves of (c) 1st cycle, 2nd cycle and 10th cycle at 0.5 C from 0.01 to 3 V and (d) 1st cycle, 100th cycle, 200th and 400th cycle at 0.5 C from 0.01 to 3 V. (e) Cycling capacity and Coulombic efficiency profiles at 0.5 C.

4. Conclusions

Metallic 1T phase MoS_2 nanosheets and 2H MoS_2 were synthesized by a facile eco-friendly alkali metal hydroxide-assisted controlled and targeted approach via calcination of lithium hydroxide and ammonium tetrathiomolybdate under argon atmosphere at 1000 °C and 400 °C, respectively. 1T MoS_2 single crystal nanosheets were used as lithium anodes, presenting superior electrochemical performances including long cycle life and high capacities. The 1T MoS_2 electrode presented first charge and discharge capacities are up to 889.1 mAh g^{-1} and 892.5 mAh g^{-1} , respectively. In 400th cycle, the charge and discharge capacities were still 737.2 mAh g^{-1} and 738.0 mAh g^{-1} , respectively, with 82.9% capacity retention ratio. The work not only provides a novel strategy for fabricating metallic 1T phase MoS_2 which are used as lithium ion battery anodes, but introduce a facile eco-friendly facile lithium hydroxide-assisted controlled and targeted approach for different phase MoS_2 (1T and

2H), also it can be extended to other alkali metal hydroxide-assisted (NaOH, KOH) approaches for MoS₂ preparation.

Conflicts of interest

There are no conflicts to declare.

Acknowledgments

This work at the University of Illinois at Urbana-Champaign was supported by the National Science Foundation Engineering Research Centre for Power Optimization of Electro-Thermal systems (POETS) with cooperative agreements EEC-1449548.

The author gratefully acknowledges Professor Paul V. Braun of Department of Materials Science and Engineering, University of Illinois at Urbana-Champaign for his useful advice and the use of his laboratory for this research work. The research was carried out in the Frederick Seitz Materials Research Laboratory Central Research Facilities, University of Illinois at Urbana-Champaign. The authors are deeply thankful to Dr. Richard T. Haasch for XPS measurements. Zhao Li also acknowledges China Scholarship Council during his visit to the University of Illinois at Urbana-Champaign.

References

- [1] R. Wang, S. Wang, Y. Zhang, D. Jin, X. Tao, L. Zhang, *Nanoscale*, 2018, **10**, 11165-11175.
- [2] J. Pei, H. Geng, E. H. Ang, L. Zhang, X. Cao, J. Zheng, H. Gu, *Nanoscale*, 2018, **10**, 17327-17334.
- [3] Y. Zhang, T. He, G. Liu, L. Zu, J. Yang, *Nanoscale*, 2017, **9**, 10059-10066.
- [4] X. Xie, T. Makaryan, M. Zhao, K.L. Van Aken, Y. Gogotsi, G. Wang, *Adv. Energy Mater.*, 2016, **6**, 1502161.
- [5] Y. Liu, J. Wu, K.P. Hackenberg, J. Zhang, Y.M. Wang, Y. Yang, K. Keyshar, J. Gu, T. Ogitsu, R. Vajtai, J. Lou, P.M. Ajayan, Brandon C. Wood, B.I. Yakobson, *Nat. Energy* 2017, **6**, 17127.
- [6] J. Zhu, Z.C. Wang, H. Dai, Q. Wang, R. Yang, H. Yu, M. Liao, J. Zhang, W. Chen, Z. Wei, N. Li, L. Du, D. Shi, W. Wang, L. Zhang, Y. Jiang, G. Zhang, *Nat. Commun.*, 2019, **10**, 1348.
- [7] J. Li, H. Zhao, J. Wang, N. Li, M. Wu, Q. Zhang, Y. Du, *Nano Energy*, 2019, **62**, 876-882.
- [8] M. Chhowalla, H.S. Shin, G. Eda, L.J. Li, K.P. Loh, H. Zhang, *Nat. Chem.*, 2013, **5**, 263-275.
- [9] Z. Lei, J. Zhan, L. Tang, Y. Zhang, Y. Wang, *Adv. Energy Mater.*, 2018, **8**, 1703482.
- [10] X. Geng, W. Sun, W. Wu, B. Chen, A. Al-Hilo, M. Benamara, H. Zhu, F. Watanabe, J. Cui, T.P. Chen, *Nat. Commun.*, 2016, **7**, 10672.
- [11] A. Gigot, M. Fontana, M. Serrapede, M. Castellino, S. Bianco, M. Armandi, B. Bonelli, C.F. Pirri, E. Tresso, P. Rivolo, *ACS Appl. Mater. Interfaces*, 2016, **8**, 32842-32852.
- [12] M. Acerce, E.K. Akdogan, M. Chhowalla, *Nature*, 2017, **549**, 370-373.
- [13] X. Geng, Y. Jiao, Y. Han, A. Mukhopadhyay, L. Yang, H. Zhu, *Adv. Funct. Mater.*, 2017, **27**, 1702998.
- [14] M. Acerce, D. Voiry, M. Chhowalla, *Nat. Nanotech.*, 2015, **10**, 313-318.
- [15] Y. Fang, J. Pan, J. He, R. Luo, D. Wang, X. Che, K. Bu, W. Zhao, P. Liu, G. Mu, H. Zhang, T. Lin, F. Huang, *Angew. Chemie*, 2018, **57**, 1232-1235.
- [16] M. Wang, L. Fan, D. Tian, X. Wu, Y. Qiu, C. Zhao, B. Guan, Y. Wang, N. Zhang, K. Sun, *ACS Energy Lett.*, 2018, **3**, 1627-1633.
- [17] C. Zhao, J.M. Ang, Z. Liu, X. Lu, *Chem. Eng. J.*, 2017, **330**, 462-469.
- [18] M. Wu, J. Zhan, K. Wu, Z. Li, L. Wang, B. Geng, L. Wang, D. Pan, *J. Mater. Chem. A*, 2017, **5**, 14061-14069.
- [19] W. Zhou, *Nat. Nanotech.*, 2014, **9**, 333-334.
- [20] R. Kappera, D. Voiry, S.E. Yalcin, B. Branch, G. Gupta, A.D. Mohite, M. Chhowalla, *Nat. Mater.*, 2014, **13**, 1128-1134.
- [21] Y. Chen, Z. Fan, Z. Zhang, W. Niu, C. Li, N. Yang, B. Chen, H. Zhang, *Chem. Rev.*, 2018, **118**, 6409-6455.
- [22] D. Wang, Y. Xiao, X. Luo, Z. Wu, Y.-J. Wang, B. Fang, *ACS Sustainable Chem. Eng.*, 2017, **5**, 2509-2515.
- [23] X. Zhang, Z. Lai, C. Tan, H. Zhang, *Angew. Chemie*, 2016, **55**, 8816-8838.
- [24] T. Xiang, Q. Fang, H. Xie, C. Wu, C. Wang, Y. Zhou, D. Liu, S. Chen, A. Khalil, S. Tao, Q. Liu, L. Song, *Nanoscale*, 2017, **9**, 6975-6983.
- [25] Z. Deng, H. Jiang, C. Li, *Small*, 2018, **14**, 1800148.
- [26] Roy, P.; Srivastava, S. K. *Thin Solid Films*, 2006, **496**, 293-298.
- [27] H. W. Wang, P. Skeldon, G. E. Thompson, *Surf. Coat. Technol.*, 1997, **91**, 200-207.
- [28] C. Yang, Z. Chen, I. Shakir, Y. Xu, H. Lu, *Nano Res.*, 2016, **9**, 951-962.
- [29] J. Heising, M. G. Kanatzidis, *J. Am. Chem. Soc.*, 1999, **121**, 638-643.

- [30] Q. Tang, D.-e. Jiang, *Chem. Mater.*, **2015**, *27*, 3743-3748.
- [31] Y. C. Lin, D. O. Dumcenco, Y. S. Huang, K. Suenaga, *Nat. Nanotech.*, 2014, **9**, 391-396.
- [32] B. Radisavljevic, A. Radenovic, J. Brivio, V. Giacometti, A. Kis, *Nature Nanotech.*, 2011, **6**, 147-150.
- [33] G. Eda, T. Fujita, H. Yamaguchi, D. Voiry, M. Chen, M. Chhowalla, *ACS Nano*, 2012, **6**, 7311-7317.
- [34] G. Eda, H. Yamaguchi, D. Voiry, T. Fujita, M. Chen, M. Chhowalla, *Nano Lett.*, 2011, **11**, 5111-5116.
- [35] Y. Yu, G. H. Nam, Q. He, X. J. Wu, K. Zhang, Z. Yang, J. Chen, Q. Ma, M. Zhao, Z. Liu, F. R. Ran, X. Wang, H. Li, X. Huang, B. Li, Q. Xiong, Q. Zhang, Z. Liu, L. Gu, Y. Du, W. Huang and H. Zhang, *Nat. Chem.*, 2018, **10**, 638-643.
- [36] S. Wang, D. Zhang, B. Li, C. Zhang, Z. Du, H. Yin, X. Bi, S. Yang, *Adv. Energy Mater.*, 2018, **8**, 1801345.
- [37] L. Liu, J. Wu, L. Wu, M. Ye, X. Liu, Q. Wang, S. Hou, P. Lu, L. Sun, J. Zheng, L. Xing, L. Gu, X. Jiang, L. Xie, L. Jiao, *Nat. Mater.*, 2018, **17**, 1108-1114.
- [38] Y. Qi, Q. Xu, Y. Wang, B. Yan, Y. Ren, Z. Chen, *ACS Nano*, 2016, **10**, 2903-2909.
- [39] M.Z.M. Nasir, C.C. Mayorga-Martinez, Z. Sofer, M. Pumera, *ACS Nano*, 2017, **11**, 5774-5784.
- [40] H. Li, Q. Zhang, C. C. R. Yap, B. K. Tay, T. H. T. Edwin, A. Olivier and D. Baillargeat, *Adv. Funct. Mater.*, 2012, **22**, 1385-1390.
- [41] P. Cheng, K. Sun, Y.H. Hu, *Nano Lett.*, 2016, **16**, 572-576.
- [42] Y. Huang, Y. Sun, X. Zheng, T. Aoki, B. Pattengale, J. Huang, X. He, W. Bian, S. Younan, N. Williams, J. Hu, J. Ge, N. Pu, X. Yan, X. Pan, L. Zhang, Y. Wei, J. Gu, *Nat. Commun.*, 2019, **10**, 982.
- [43] Y. Yu, G.H. Nam, Q. He, X.J. Wu, K. Zhang, Z. Yang, J. Chen, Q. Ma, M. Zhao, Z. Liu, F.R. Ran, X. Wang, H. Li, X. Huang, B. Li, Q. Xiong, Q. Zhang, Z. Liu, L. Gu, Y. Du, W. Huang, H. Zhang, *Nat. Chem.* 2018, **10**, 638-643.
- [44] X. Geng, Y. Zhang, Y. Han, J. Li, L. Yang, M. Benamara, L. Chen, H. Zhu, *Nano Lett.*, 2017, **17**, 1825-1832.
- [45] H. Wang, Z. Lu, S. Xu, D. Kong, J.J. Cha, G. Zheng, P.C. Hsu, K. Yan, D. Bradshaw, F.B. Prinz, Y. Cui, *Proc. Natl. Acad. Sci.*, 2013, **110**, 19701-19706.
- [46] U.K. Sen, P. Johari, S. Basu, C. Nayak, S. Mitra, *Nanoscale*, 2014, **6**, 10243-10254.
- [47] S. Xia, Y. Wang, Y. Liu, C. Wu, M. Wu, H. Zhang, *Chem. Eng. J.* 2018, **332**, 431-439.